Journal of Solid State Chemistry **168,** 306–315 (2002)
doi:10.1006/jssc.2002.9630

The Superstructure of Lead Tetragonal Tungsten Bronze

Sarah K. Haydon and David A. Jefferson[1]

Department of Chemistry, Centre for Atomic Imaging, University of Cambridge, Lensfield Road, Cambridge CB2 1EW, United Kingdom

Received November 5, 2001; in revised form April 19, 2002; accepted May 2, 2002

Electron-optical studies of the superstructure of lead tetragonal tungsten bronze (lead-TTB) are presented. Samples were synthesized for a range of lead compositions and synthesis conditions. For lead-TTB synthesized for very short reaction times, compositional analysis combined with electron diffraction revealed these specimens to also contain significant levels of an intergrowth tungsten bronze (ITB) phase. It was proposed that ITB was formed during the reaction as an intermediate between the tungsten oxide reagent and lead-TTB. Electron-diffraction investigations of lead-TTB over a range of specimen compositions determined that the large majority of crystallites examined exhibited a well-ordered $2\sqrt{2}a_{\mathrm{TTB}}\times\sqrt{2}b_{\mathrm{TTB}}\times 2c_{\mathrm{TTB}}$ supercell periodicity, although evidence of a larger *a*-axis repeat was also observed. No evidence for a variation in the supercell with lead composition was observed. A model for the supercell was generated from consideration of stacking sequences of correlated ordered arrays of lead and tilted octahedra and it was demonstrated that larger superstructures could be generated using alternative stacking sequences. © 2002 Elsevier Science (USA)

Key Words: **HREM; electron diffraction; octahedral tilt; supercell; lead tetragonal tungsten bronze; pentagonal tunnels; stacking sequences.**

1. INTRODUCTION

Tungsten oxide bronzes are formed when tungsten (VI) oxide, WO_3, is reduced, normally by exposure to the vapor of a guest or 'impurity' metal (*M*). This reaction induces the oxide framework to distort or rearrange to incorporate the guest atoms, and a non-stoichiometric compound, M_xWO_3, is formed. There are several possible resulting bronze structures possessing either square (1), a combination of square and pentagonal (2) or hexagonal (3, 4) tunnels, whose configuration depends on the size and quantity of the guest metal incorporated. For certain guest metal species (5), however, the structure formed is a tetragonal array of pentagonal tunnels (PTs) of WO_6 octahedra and the basic structure of 'tetragonal tungsten bronze' (TTB) (2) is shown in Fig. 1a. The formation of TTB from the WO_3 parent oxide is envisaged by the operation of a rotary crystallographic shear on the framework (6, 7). PTs provide a site for the host reducing species to reside and stabilize the new framework structure.

The TTB structure is found for only a few guest metal species (Na, K, Ca, Ba, Sn and Pb) (5) and of these sodium- (8), tin- (9, 10), and most recently lead-TTB (11), have been found to possess true unit cells based on $\sqrt{2}\mathbf{a}_{\mathrm{TTB}}\times\sqrt{2}\mathbf{a}_{\mathrm{TTB}}\times 2\mathbf{c}_{\mathrm{TTB}}$ ('$\sqrt{2}\times\sqrt{2}\times 2$') superstructures of the basic TTB unit. The formation of these supercells has been linked to WO_6 octahedral framework distortion, and for tin- and lead-TTB, a possible ordering amongst guest metal tunnel occupants. Superlattices are also common in fully oxidized ternary oxides which are also based on the TTB structure, such as $Nb_8W_9O_{47}$ (12) and $Nb_4W_7O_{31}$ (13, 14), and the origin of these has been explored in a related study (15).

The average structure of $Pb_{0.26}WO_3$ determined by Triantafyllou *et al.* (11) using single-crystal X-ray diffraction is shown in Fig. 1b. This study revealed that all equatorial oxygens (O3, O4 and O5) were split along the **c**-axis in a two-fold manner, implying a puckering of the equatorial oxygen network with respect to the **ab** plane of the cell. In addition, the $W(2)O_6$ octahedron was found to be tilted from the **c**-axis along the [110] direction of the basic cell. Selected area electron diffraction (SAED) revealed the formation of a tetragonal, I-centered $\sqrt{2}\times\sqrt{2}\times 2$ supercell, which was explained by a system of cooperatively tilted $W(2)O_6$ octahedra. Additional superstructure reflections not indexed by the $\sqrt{2}\times\sqrt{2}\times 2$ cell were attributed to an additional modulated structure formed by a periodic repetition of domains of the $\sqrt{2}\times\sqrt{2}\times 2$ supercell related by anti-phase boundary planes. If the overall periodicity of the superstructure is denoted by $\mathbf{a}_{\mathrm{ss}}$, its value in this structure was reported as $(5\sqrt{2}/2)\mathbf{a}_{\mathrm{TTB}}$. Lead was found to be distributed over three off-center sites within the PTs (occupancies Pb(1*A*), 0.55;

[1]To whom correspondence should be addressed. Fax: +44-1223-336-362. E-mail: daj4@cus.cam.ac.uk.

0022-4596/02 $35.00

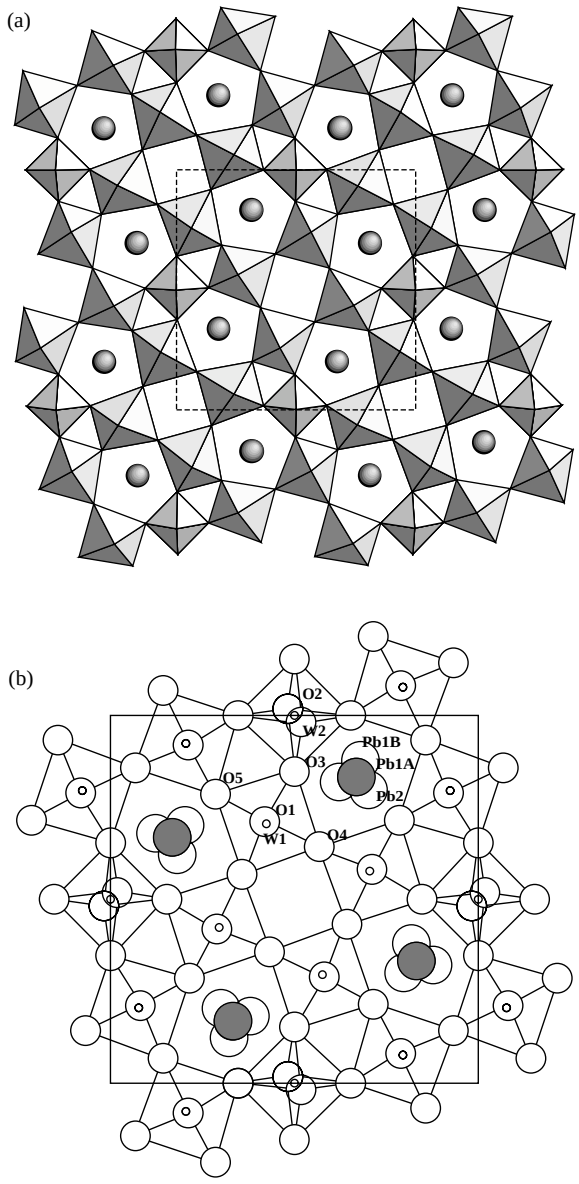

FIG. 1. (a) The [001] projection of the idealized crystal structure of TTB, $\mathbf{a} = \mathbf{b} \approx 12$ Å, $\mathbf{c} \approx 3.8$ Å, with the black balls representing the lead atoms within the pentagonal tunnels and the shaded polyhedra the WO_3 octahedra. (b) The average structure of $Pb_{0.26}WO_3$ determined by Triantfyllou *et al.* (11), $\mathbf{a}_{av} = \mathbf{b}_{av} = 12.2$ Å, $c_{av} = 3.8$ Å. The shaded circle highlights the position of the principle lead site, Pb1*A*.

Pb(1*B*), 0.03; and Pb(2), 0.04) in an analogous manner to that previously reported for $Sn_{0.3}WO_3$ (10). Similar PT cation splitting was found in studies of the ferroelectric TTB-related compound $PbNb_2O_6$ (16, 17) and the effect has been attributed to the lone pair stereoactivity of Pb^{2+} and Sn^{2+} (10, 11, 16, 17). In an idealized structure, the cation at the center of a PT will be in 10-fold coordination, being in the middle of a pentagonal prism, but as noted by Steadman (9), cation displacement from the center of the PT is stabilized by its coordination with the surrounding oxygen framework. Such a movement brings the cation much closer to four of the coordinating oxygen atoms, being therefore at the apex of a pyramid, which is similar to the coordination found in PbO and SnO (18).

It was suggested by Triantafyllou *et al.* (11) that the lead-TTB superstructure and modulation reflections could also be attributable to lead ordering over the three sites within each PT, and that octahedral tilt and lead ordering could be correlated effects. With this possibility in mind, and since Triantafyllou *et al.* (11) investigated the supercell for a single composition, this paper presents an electron-optical investigation into the effect on the superstructure of lead concentration and variation in synthesis conditions.

Lead-TTB, Pb_xWO_3, was first prepared by Bernoff and Conroy (19), who reported its formation in the composition range $0.16 \leq x \leq 0.35$ for samples heated at 1150–1200°C. In subsequent work, Ekström and Tilley (20) used high-resolution electron microscopy (HREM) and SAED to investigate phases formed for compositions between $0.01 \leq x \leq 0.28$. For samples prepared at 1100°C, their results were in general agreement with those previously reported (19) and lead-TTB was observed for compositions with $x > 0.18$, coexisting with WO_3 for compositions below this. For preparations in the range $0.01 < x < 0.18$ prepared at lower temperatures (700–1000°C), the coexistence of lead-TTB and/or WO_3, with a range of lead intergrowth tungsten bronzes (lead-ITBs) was reported. Lead-ITB was determined to be the only phase type for compositions in the range $0.03 < x < 0.05$, and the structure of $Pb_{0.04}WO_3$ was subsequently determined to be composed of single rows of hexagonal tunnels separated by slabs of corner-sharing WO_6 octahedra (21).

2. EXPERIMENTAL

Samples of lead-TTB were prepared from the appropriate quantities of lead (AnalaR, 99.97%) and WO_3 (Johnson Matthey, 99.8%). Ground and homogenized mixtures were encapsulated in evacuated silica ampoules and heated at high temperatures before being cooled slowly. Samples were prepared for compositions $x = 0.1$, 0.175, 0.225 and 0.3, heating at 1000°C for 1 h, and for compositions $x = 0.15$ and 0.4, heating at 900°C for 6 days. After reaction, all specimens prepared were very dark blue–black polycrystalline powders with a metal-like appearance when ground under acetone. No residual lead was detected in any specimen; however, in the $x = 0.3$ sample, fine needles were observed on the sides of the silica tube. When viewed with an optical microscope, these were opaque and appeared to have grown in bunches, which is in agreement with the reported lead-TTB crystal morphology (20).

Characterization was performed using powder X-ray diffraction (PXRD), HREM, SAED and energy-dispersive

X-ray spectroscopy (EDS). PXRD studies employed a Stoe horizontal diffractometer working in transmission mode (Cu$K\alpha$, $\lambda = 1.5456$ Å). For the diffractometer, small quantities of each sample were mounted on transparent adhesive tape, which was inserted in a disk-like holder. Images and SAED patterns were recorded using a JEM-200CX electron microscope with an ultra-high-resolution specimen stage and objective lens ($C_S = 0.36$ mm, $C_C = 0.65$ mm) (22, 23) operated at 200 kV. Image simulations were performed using customized software (24). Specimens for microscopy were first embrittled under liquid N_2 and subsequently ground in acetone suspension. A drop of this was dispersed on a holey carbon film supported on a standard gold specimen grid. Quantitative EDS measurements were recorded using a PGT beryllium window detector, fitted to a standard JEM-2010 electron microscope ($C_S = 0.50$ mm, $C_C = 1.10$ mm). The detector was calibrated using a previously prepared standard of $PbWO_4$, in order to determine the detector efficiency for the W$L\alpha$ and Pb$L\alpha$ lines.

The homogeneity of the $PbWO_4$ standard was initially checked by PXRD, but in order to obtain reasonable statistics and to check further the homogeneity of the material, 50-point analyses were obtained. The effects of absorption errors were monitored by noting the value of the intensity ratio for the WM and W$L\alpha$ lines in the spectra, and where this value was abnormally low the measurement was not included in the final determination. Similarly, any analyses with W$L\alpha$/Pb$L\alpha$ intensity ratios differing markedly from the norm were also rejected. The final standard deviation in this intensity ratio for the standard was $\pm 4.0\%$. Between 35 and 50 analyses were obtained for each unknown specimen studied, and the same absorption criterion was applied.

3. RESULTS AND DISCUSSION

3.1. Characterization Results

PXRD patterns were recorded from the samples and all major lines could be indexed on the average lead-TTB cell (Fig. 1b). This confirmed the formation of lead-TTB for the whole range of stoichiometries prepared. No evidence was found for additional lines in the patterns caused by a doubled-**c**-axis superstructure, but weak WO_3 and lead tungstate ($PbWO_4$) reflections were observable for compositions prepared at 1000°C. Some of these patterns also contained very weak reflections not capable of being indexed as either lead-TTB, WO_3 or $PbWO_4$ (see below). Comparison of the PXRD patterns from specimens $x = 0.15$ and 0.4 heated at 900°C for 6 days found that the $x = 0.4$ sample contained only lead-TTB and a trace amount of $PbWO_4$. The $x = 0.15$ pattern also displayed peaks from these phases, however, additional reflections indexed to WO_3 were also observed.

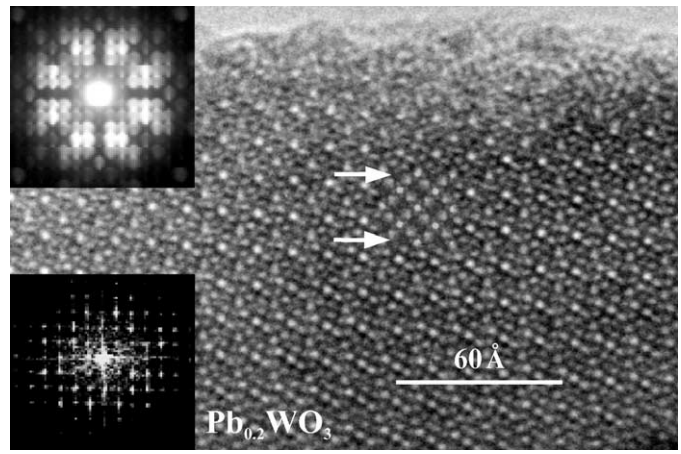

FIG. 2. A [001] projection HREM image of lead-TTB with power spectrum, SAED pattern and image simulation inset (crystal thickness = 50 Å, $\Delta f = -500$ Å).

HREM confirmed the formation of lead-TTB for all compositions and a typical [001]-axis projected image, image power spectrum (PS) and SAED pattern are shown in Fig. 2. The presence of residual WO_3 in some samples was confirmed by the observation of SAED patterns from a WO_3 phase exhibiting characteristic crystallographic shear planes (25) and a more complex, PC-type reduced oxide, $W_{22}O_{68}$ (26). These reduced phases presumably account for the weak unidentified reflections in some PXRD patterns, although these lines were of such low intensity that exact assignment was not possible.

The results of a quantitative EDS study on samples with $x = 0.1$, 0.15, 0.225, 0.3 and 0.4 are listed in Table 1. Readings from $PbWO_4$ have been omitted. These data show that for all samples heated at 1000°C for 1 h, measurements could be consistently grouped into three types. Principally, the majority of readings corresponded to an average composition which was approximately the nominal value. A further group of measurements showed a significant lead content but one that was substantially less than that expected from the nominal value. Finally, a third group could be made of measurements where no lead signal was detected and clearly corresponded to the small quantities of residual WO_3 and/or reduced oxides detected by PXRD.

The high lead content groupings were proven to correspond to lead-TTB by recording asymmetric SAED patterns from some crystals at the time of EDS analysis, as shown in Fig. 3. The range of stoichiometries observed for the low lead content readings, $0.02 \leq x \leq 0.04$, were characteristic of the formation of lead-ITB. Both low and high lead composition readings were observed to come from long needle-like crystals that lay flat on the surface of

TABLE 1
EDS Results for the Series of Lead-TTB Preparations

Nominal composition	Experimental composition	Synthesis
$Pb_{0.1}WO_3$	Pb = 0.16 ± 0.02 Pb = 0.04 ± 0.02 Pb = 0.00 ± 0.03	1000°C/1 h
$Pb_{0.15}WO_3$	Pb = 0.16 ± 0.02 Pb = 0.02[a]	900°C/6 days
$Pb_{0.225}WO_3$	Pb = 0.19 ± 0.03 Pb = 0.04 ± 0.03 Pb = −0.01 ± 0.01	1000°C/1 h
$Pb_{0.3}WO_3$	Pb = 0.23 ± 0.13 Pb = 0.03 ± 0.01 Pb = −0.01 ± 0.02	1000°C/1 h
$Pb_{0.4}WO_3$	Pb = 0.33 ± 0.03	900°C/6 days

[a] The average value of two readings.

the supporting grid in the electron microscope. In order to determine if the structure of needles with high and low lead contents were distinct, after compositions were determined by EDS, needle crystals were tilted about an axis parallel to their length and SAED patterns were recorded.

Fig. 4 shows example SAED patterns and corresponding individual compositions from three needle crystals in sample $x = 0.3$. Figure 4a shows a SAED pattern obtained from a high lead content needle. The reciprocal lattice ratio (y/x) for this pattern was determined as 0.88, which agrees with the value for the lead-TTB doubled cell of $\sqrt{2}\mathbf{a}^*_{TTB}/(2\mathbf{c})^*_{TTB} = 0.88$, calculated using the average TTB cell parameters $\mathbf{a}_{TTB} = 12.2$ Å and $2\mathbf{c}_{TTB} = 7.6$ Å (11). This implies that the y distance corresponds to the $\sqrt{2}\mathbf{a}^*_{TTB}$ repeat along $[110]_{TTB}$ and x the $(2\mathbf{c})^*_{TTB}$ repeat along $[001]_{TTB}$, and confirms the doubled-**c** periodicity supercell of lead-TTB reported previously (11). Figure 4a also demonstrates the differing periodicity of the odd-order Laue layers with respect to even-order ones, where a triplet of spots (the central one somewhat diffuse) coincides with the corners of the basic $\sqrt{2}\mathbf{a}^*_{TTB}$ cell repeat of TTB observable on even-order layers. Maxima on both the odd- and even-order Laue layers in Fig. 4a also show evidence of streaking, which is indicative of disorder in the structure of this crystallite.

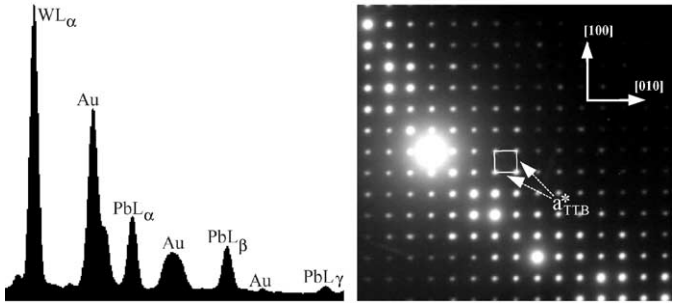

FIG. 3. An example EDS spectrum of lead-TTB (gold supporting grid) and corresponding asymmetric SAED pattern from sample $Pb_{0.4}WO_3$. Approximate axial directions are indicated. Individual crystal composition: Pb = 0.29.

Figures 4b and 4c display SAED patterns from two low lead content needles, where a halved periodicity in Laue layers perpendicular to the axis of the needle (direction x) can be observed. In Fig. 4b, reflections in adjacent Laue layers are aligned, and the reciprocal lattice ratio was calculated as 0.28. Assuming a single **c**-axis repeat of 3.8 Å, the periodicity along direction y was calculated as approximately 13 Å. In Fig. 4c, however, reflections on odd-numbered rows parallel to the long axis occur exactly half-way between the equivalent positions on even-numbered rows, and the reciprocal lattice ratio is smaller at 0.23. These findings support the compositional evidence for the formation of an ITB phase, since the ≈13 Å repeat is compatible with a '3'-type structure, shown in Fig. 5a, where the separation of the rows of tunnels is three WO_6 octahedra wide. The idealized 3-ITB structure has a C-centered orthorhombic unit cell with dimensions of **a** = 28, **b** = 7.5 and **c** = 3.9 Å, however, due to the C-centering, the reciprocal lattice of this odd-numbered ITB appears oblique in projections of the **ab** plane but rectangular in projections down the [010]-axis with an apparently halved **a**-axis repeat of 14 Å.

Simulated SAED patterns were generated from the 3-ITB model using customized software (24), and [010] and [011] projection patterns are shown in Figs. 5b and 5c. Reflections in adjacent layers of the [010] pattern are aligned and the reciprocal lattice ratio agreed with that determined for the experimental pattern in Fig. 4b. The C-centered nature of the cell is evident in the [011] simulation and reflections in adjacent layers are oblique. The reciprocal lattice ratio of this projection was also in close agreement with that calculated for the experimental pattern (Fig. 4c). It is probable therefore that the low lead readings from the quantitative EDS study can be attributed to the formation of a 3-type lead-ITB phase. The faint streaking of reflections along **a*** in Fig. 4c suggests that the ITB is disordered, since ITBs can exhibit variations in the separation of the tunnels (20).

Ekström and Tilley (20) reported the formation of lead-ITBs in the range $n = 6-12$ in samples with compositions $0.01 < x < 0.18$ heated at 700–1000°C for prolonged periods. EDS results for samples $x = 0.15$ and 0.4, which were synthesized using similar conditions agree with their HREM investigation (except for the observation of $PbWO_4$ in this study). Lead-TTB and a small quantity of lead-ITB was detected for the $x = 0.15$ composition (two out of 50 measurements), whereas only lead-TTB was

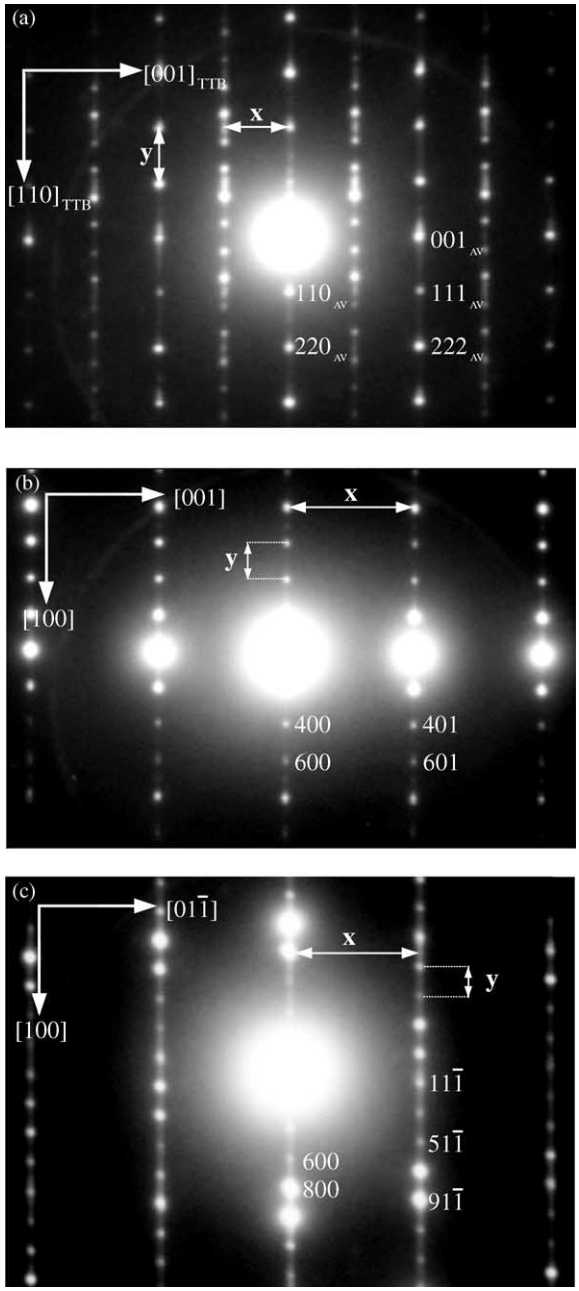

FIG. 4. Example needle crystal SAED patterns from $Pb_{0.3}WO_3$. All patterns recorded at a camera length of 80 cm. (a) [−110] projection of lead-TTB, indexed with respect to the average TTB cell shown in Fig. 1b. Needle composition: Pb = 0.18. (b) [010] projection of 3-ITB. Needle composition: Pb = 0.01. (c) [011] projection of 3-ITB. Needle composition: Pb = 0.06. (b) and (c) are indexed with respect to the idealized orthorhombic **a** = 28, **b** = 7.5 and **c** = 3.9 Å cell of 3-ITB shown in Fig. 5a. Compositions are within the error of the EDS analysis (Table 1).

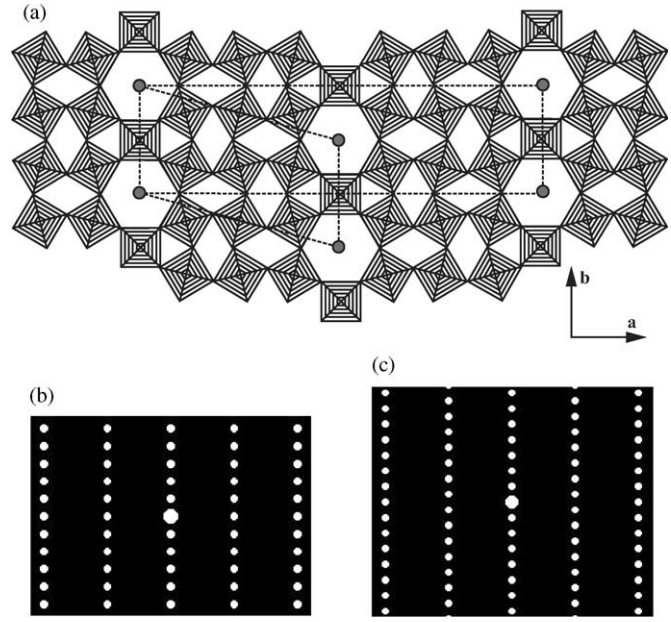

FIG. 5. (a) The idealized structure model of orthorhombic 3-ITB (monoclinic cell indicated). Orthorhombic unit cell: **a** = 28 Å, **b** = 7.5 Å and **c** = 3.8 Å.Simulated SAED patterns for (b) the [010] (reciprocal lattice ratio = 0.28) and (c) [011] directions (reciprocal lattice ratio = 0.24) of 3-ITB.

found in the $x = 0.4$ sample. EDS did not detect WO_3 in the $x = 0.15$ sample, hence, the extra reflections in the PXRD pattern for this sample, originally assigned to WO_3, must actually be due to lead-ITB phases since ITBs exhibit PXRD patterns similar to WO_3 itself (20). This work also reports the formation of lead-ITB in samples heated at 1000°C with a reduced tunnel separation, which persist at much higher nominal specimen compositions than that is found by Ekström and Tilley (20) (Table 1). It is probable that this is as a result of the short synthesis conditions employed for these specimens and it seems likely that the ITB forms as a metastable intermediate between WO_3 and lead-TTB.

The EDS results indicate a lower limit of stability for lead-TTB of $Pb_{0.16}WO_3$, which is in good agreement with that reported in other work (19, 20).

3.2. Electron Diffraction

Asymmetric (or off-axis) SAED patterns recorded from all lead-TTB compositions displayed systematically weak odd-order Laue layers lying half-way between the positions of the strong even-order layers corresponding to the basic 3.8 Å $\mathbf{c}_{TTB}$ repeat. An example pattern from sample $Pb_{0.175}WO_3$ is shown in Fig. 6a. For even-numbered Laue zones, the $\mathbf{a}^*$ and $\mathbf{b}^*$ lattice repeat distances correspond to the basic TTB cell, and the supercell is only apparent on odd order layers. This confirmed observations made from TTB needle crystals during the compositional analysis (Fig. 4a). The enlarged SAED pattern, shown in Fig. 6b, indicates that the supercell periodicity along $[110]_{TTB}$ is four times that of the average structure. A second SAED pattern from this crystal at another tilt-angle confirmed the

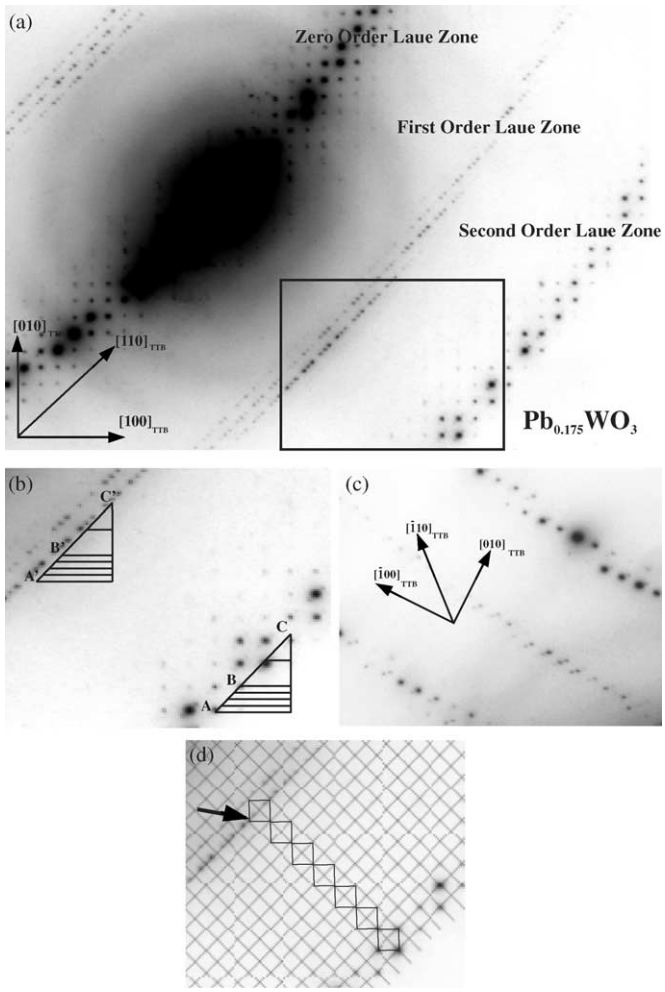

FIG. 6. (a) An asymmetric (off-axis) SAED pattern from sample $Pb_{0.175}WO_3$. (b) An enlarged area of (a) [shown by a black box in (a)] demonstrating that the periodicity of the superstructure reflections is four times that of the average structure. Distance $AC = A'C' = 3\sqrt{2}\mathbf{a}^*_{TTB}$, and $AB = A'B' = 4(\sqrt{2}/4)\mathbf{a}^*_{TTB}$. (c) An enlargement of a second SAED pattern from the same crystal, but tilted off-axis in a different direction. (d) The enlargement shown in (b), with a black mesh defining the reciprocal lattice and staggered squares illustrating the position of the basic TTB cell repeat with respect to the $2\sqrt{2} \times \sqrt{2} \times 2$ cell. Approximate axial directions are indicated on the SAED patterns.

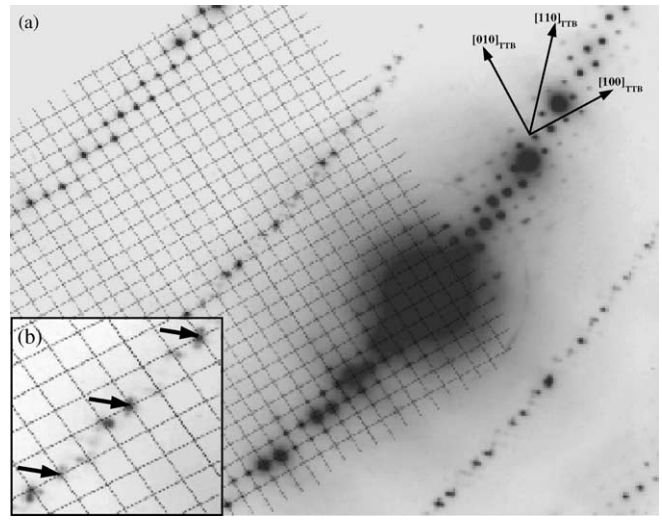

FIG. 7. (a) A SAED pattern from sample $Pb_{0.4}WO_3$ displaying a larger $\mathbf{a}_{ss}$ periodicity. Approximate axial directions are indicated. (b) An enlargement of (a) where the black mesh defines the TTB reciprocal lattice. The arrows indicate that the corners of the basic TTB cell coincide with the center of the triplets of superstructure reflections. Evidence for the twinning of the superstructure in this crystal is also evident in (b).

periodicity along $[-110]_{TTB}$ (Fig. 6c), indicating overall supercell dimensions of: $\mathbf{a}_{ss} = 2\sqrt{2}\mathbf{a}_{TTB}$, $\mathbf{b}_{ss} = \sqrt{2}\mathbf{a}_{TTB}$ and $\mathbf{c}_{ss} = 2\mathbf{c}_{TTB}$, i.e., a '$2\sqrt{2} \times \sqrt{2} \times 2$' supercell. It was also found that the strongest maxima on successive Laue zones do not superimpose, as shown in the enlargement of Fig. 6d.

For reactions at 1000°C, only the $2\sqrt{2} \times \sqrt{2} \times 2$ supercell was observed and for those at 900°C, the $2\sqrt{2} \times \sqrt{2} \times 2$ type was also most common, but a larger $\mathbf{a}_{ss}$ periodicity was found for one crystal in sample $Pb_{0.4}WO_3$ (Fig. 7a). The $\sqrt{2}\mathbf{a}_{TTB}$ $\mathbf{b}_{ss}$-axis repeat, however, remained constant in all patterns analyzed. Evidence for twinning of the supercell is also observed in Fig. 7b. The occurrence of this pattern indicates that even larger superlattice periodicities may be developed in certain cases.

The lead-TTB needle-crystal SAED pattern (Fig. 4a) suggested that the center spot of the triplet of superstructure reflections on odd-order layers coincides with the corners of the basic $\sqrt{2}\mathbf{a}^*_{TTB}$ cell repeat of TTB observable on even-order layers. This was supported by the analysis of asymmetric SAED patterns using a method devised to interpret reciprocal lattice periodicities in adjacent Laue levels of asymmetric SAED patterns (15, 27). Examples of this analysis are shown in Figs. 6d and 7b.

3.3. Discussion

The results of this study provide no evidence for a variation in the supercell with lead composition. The $2\sqrt{2} \times \sqrt{2} \times 2$ structure was formed for all compositions prepared, with the exception of one crystal analyzed in the $Pb_{0.4}WO_3$ sample. This occurrence is perhaps more likely due to the long synthesis conditions employed for this specimen. Triantafyllou *et al.* (11) synthesized lead-TTB at 1100°C for 7 days and a $(5\sqrt{2}/2) \times \sqrt{2} \times 2$ structure was formed, hence, it is possible that longer heating times result in more complex ordering sequences although further work is needed to confirm this hypothesis.

This evidence implies therefore that lead ordering is not directly involved in the formation of the supercell for lead-TTB. This conclusion is supported by the observed occupancies of the lead-TTB sites in the study of

$Pb_{0.26}WO_3$ (11); virtually, all lead is located at a single position, Pb(1*A*), and the occupancies of Pb(1*B*) and Pb(2) positions are insignificant. For lead ordering over the three cation positions, a significant population of each site would be expected. Lead ordering is also difficult to reconcile with a non-stoichiometric compound such as lead-TTB where a range of lead compositions must be tolerated. However, the evidence from the single-crystal study (11) for the displacement of the main cation position, Pb(1*A*), towards the tilted $W(2)O_6$ octahedron and its known favored geometry, suggests that lead instead provides a reinforcement and stabilization of the distorted anion lattice.

The results of the single-crystal study (11) imply that generally, for moderate compositions, lead can be assumed to be situated on one site within the PTs (Pb1*A*) with an occupancy of approximately 0.5. Fig. 8 shows the effect of tilting $W(2)O_6$ on the size of the associated PTs. The tilt of one octahedron away from the lead atom site and the opposing tilt of the second produces pairs of PTs in the same layer that have differing sizes. If an average lead occupancy of 0.5 is assumed, then it is favorable for pairs of atoms to be in staggered positions parallel to the **c**-axis. This fits well with the disposition of tilts since octahedra can be imagined to 'clamp' around each filled lead position. The favored square-based pyramid coordination (9) is highlighted in Fig. 8.

The formation of a supercell that is consistent with the observed reciprocal lattice can be explained by considering stacking sequences of the basic structure. The TTB framework can be thought of as composed of strips of four corner-sharing WO_6 units that are linked by units composed of the tilted octahedra and lead atoms ('$PbWO_6$' units, Fig. 9a). If octahedral tilt is assumed to be correlated with the occupancy of PTs, and if the octahedra are tilted away from the lead atoms, then there are only two simple arrangements of the octahedron and lead atoms that maintain a $\mathbf{b}_{ss}$-axis repeat of $\sqrt{2}\mathbf{a}_{TTB}$ (denoted by A and B). These arrangements form strips of TTB that can be assembled in different ways. The most simple sequence is generated when only one arrangement of $PbWO_6$ units is used, i.e., AAAAA… or BBBBB… (Fig. 9b). This sequence produces an $\mathbf{a}_{TTB} \times \mathbf{a}_{TTB} \times 2\mathbf{c}_{TTB}$-type cell that is not truly tetragonal. Another sequence can be generated by stacking A and B units alternately (Fig. 9c). This produces a cell equivalent to the I-centered $\sqrt{2} \times \sqrt{2} \times 2$ model reported in previous TTB-bronze studies (8–11). The next logical sequence is AABBAABB… (Fig. 9d). This ordering produces the cell type required, an orthorhombic B-centered $2\sqrt{2} \times \sqrt{2} \times 2$ structure.

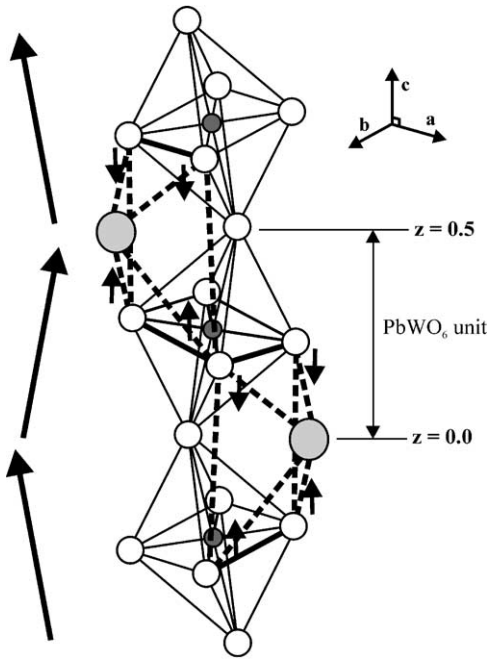

FIG. 8. Diagram illustrating the effect of tilting octahedra on the size of PTs. Light gray = lead, dark gray = tungsten, and white = oxygen.

3.4. Structure Factor Calculations

The $2\sqrt{2} \times \sqrt{2} \times 2$ model contains eight units of the average structure of lead-TTB cenetred at positions $(0,0,0)$, $(\frac{1}{2},0,0)$, $(\frac{1}{4},\frac{1}{2},0)$, $(\frac{3}{4},\frac{1}{2},0)$, $(0,0,\frac{1}{2})$, $(\frac{1}{2},0,\frac{1}{2})$, $(\frac{1}{4},\frac{1}{2},\frac{1}{2})$, $(\frac{3}{4},\frac{1}{2},\frac{1}{2})$ hence:

$$F_W(hkl) = \sum_1^{N_w/8} f_w \exp 2\pi i(hx_w + ky_w + lz_w)[1 + \exp \pi i(l)] \\ [1 + \exp \pi i(h)][1 + \exp \pi i(h/2 + k)],$$

where N_w is the number of tungsten atoms. If l is odd, the first term in square brackets, i.e., $[1 + \exp \pi i(l)]$, will be zero, and therefore tungsten atoms cannot contribute to the diffracted amplitude on odd-order Laue levels. For l even layers, however, this term will be unity, but the second term $[1 + \exp \pi i(h)]$ will be zero unless h is even. Hence, tungsten will give rise to beams only if h is even, but if k is even the third term $[1 + \exp \pi i(h/2 + k)]$ will be zero unless h is a multiple of four ($h = 4n$), and if k is odd it will vanish unless $h/2$ is odd, i.e., $h = 4n + 2$. Consequently, tungsten atom scattering contributes only to reflections on even-order layers that correspond to the basic TTB periodicity (Fig. 10a).

Equivalent $PbWO_6$ units are found at $(0,0,0)$ $(\frac{1}{2},0,\frac{1}{2})$ $(\frac{3}{4},\frac{1}{2},0)$ $(\frac{1}{4},\frac{1}{2},\frac{1}{2})$, hence the structure factor contribution from lead and oxygen can be written as

$$F_{Pb+O}(hkl) = \left\{ \sum_1^{N_{Pb}/4} f_{Pb} \exp 2\pi i(hx_{Pb} + ky_{Pb} + lz_{Pb}) \right. \\ \left. + \sum_1^{N_O/4} f_O \exp 2\pi i(hx_O + ky_O + lz_O) \right\} \\ [1 + \exp \pi i(h + l)][1 + \exp \pi i(3h/2 + k)],$$

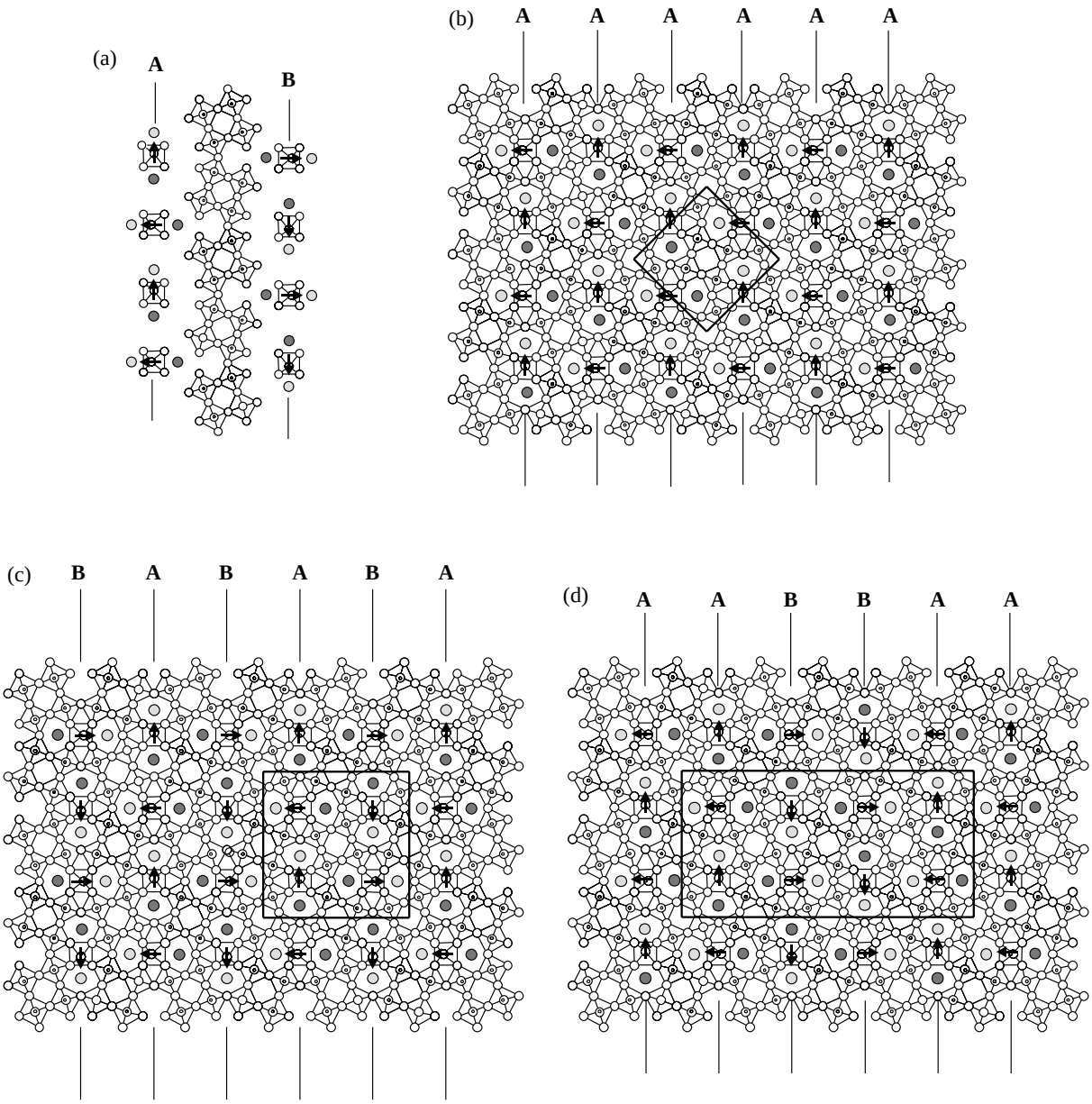

FIG. 9. (a) Possible sequences of $PbWO_6$ units. (b) The AAAAA…, (c) ABABAB… and (d) AABBAABB… stacking sequences. Light gray circles correspond to lead at $z = 0.0$, and dark gray to lead at $z = 0.5$.

where N_{Pb} and N_O are the number of lead and oxygen atoms. Considering even-order Laue layers initially, then because l is even h must also be even or the term $[1 + \exp \pi i(h + l)]$ will be zero, but the $[1 + \exp \pi i(3h/2 + k)]$ term also implies that if k is even then h must not just be even but must also be a multiple of four. Alternatively, if k is odd then $3h/2$ (h even) must be odd, i.e., $h = 4n \pm 2$. The section of reciprocal space for l is even appears the same as that shown in Fig. 10a for tungsten scattering, and lead and oxygen atoms also contribute only to maxima defining the basic TTB cell periodicity. In contrast to the tungsten scattering, however, these atoms can also contribute to the maxima on odd-order layers. For these layers, h must be odd for a beam to be present otherwise the term $[1 + \exp \pi i(h + l)]$ will vanish. In this case, therefore, the second term evaluates as $[1 + \exp \pi i(3h/2 + k)] = 1 \pm i$, for h odd irrespective of whether k is even or odd. The section of reciprocal space for odd-order Laue layers corresponding to lead and oxygen scattering is therefore shown in Fig. 10b. The net result on odd-order Laue layers

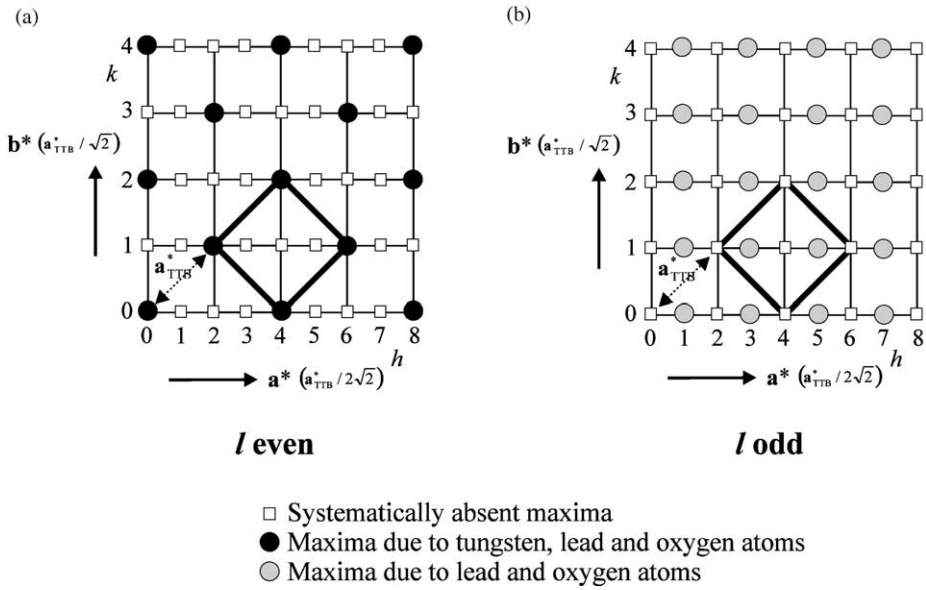

FIG. 10. (a) The even-order and (b) odd-order layer reciprocal lattice for the $2\sqrt{2} \times \sqrt{2} \times 2$ model. The black square defines the basic TTB periodicity.

is that pairs of spots are disposed either side of the (technically absent) maxima corresponding to the basic TTB cell.

This reciprocal lattice is in agreement with the experimentally observed periodicities providing that the center spot of the triplet of reflections is generated by multiple scattering. This maximum is strong in the asymmetric patterns analyzed (Figs. 6 and 7) but is absent at the origin and appears diffuse further out, as in the zone axis pattern of Fig. 4a. These observations are consistent with the effect of multiple scattering, which would be expected to be particularly severe in off-axis patterns. However, if the addition rule for multiple scattering, $(h, k, l) = (h_1 + h_2, k_1 + k_2, l_1 + l_2)$, is to hold then there are no suitable reciprocal lattice vectors in the proposed structure to generate these reflections. A more likely explanation therefore is the existence of domains of the $2\sqrt{2} \times \sqrt{2} \times 2$ sequence with structures based on other stacking possibilities, in particular the AAAAAA… or BBBBBB… types. Indeed, these structures can be formed where domains of the longer repeats meet. Structure factor calculations for these simpler models produce, in both even- and odd-order layers, reflections corresponding to the basic TTB square (as for Fig. 10a), and this therefore generates the required 'missing' reflections observed in Figs. 6 and 7.

More complex stacking sequences are possible which generate larger cells, i.e., AAABBBAAA… and these could account for the larger supercell in Fig. 7. This pattern also shows evidence of faint I-centering reflections. These can be envisaged to be as a result of intergrowths of a larger stacking sequence such as AAABBBAAA… and the ABABAB… sequence, which produces the simple I-centered $\sqrt{2} \times \sqrt{2} \times 2$ cell, at the domain boundaries.

4. CONCLUSIONS

This study provides no evidence to support the theory that the superstructure observed in lead-TTB is caused by the ordering of lead atoms within the PTs, since the superstructure(s) observed appear to be independent of lead content. Comparison of the tin- and lead-TTB studies (11), determined that the tin-TTB crystal analyzed ($Sn_{0.3}WO_3$) (10) was far more heavily distorted than the lead compound ($Pb_{0.26}WO_3$), such that faint supercell reflections were directly observed in single-crystal X-ray photographs (10). This was rationalized by consideration of the smaller size of the Sn^{2+} cation. Similar and more extensive patterns of octahedral distortion were found for the tin-TTB as well as an analogous splitting of the PT site. The distribution of the PT cation over the permitted sites was also more significant: Sn(1*A*), 0.32; Sn(1*B*), 0.06; Sn(2), 0.21, which is more supportive of a superstructure caused by a PT cation ordering scheme. A test of this hypothesis for tin-TTB would require a similar study to the one carried out here for lead-TTB to be performed.

The observation of the $2\sqrt{2} \times \sqrt{2} \times 2$ structure and a larger cell in this study, and the $(5\sqrt{2}/2) \times \sqrt{2} \times 2$ cell in other work (11), indicates that more than one ordered distortion of the TTB framework is favorable. This work has presented a logical progression for generating possible structures for lead-TTB using stacking sequences of the basic structure. The models are based on an average PT

occupancy of 0.5, but the same reciprocal lattices are produced if the lead distribution is completely random. Since lead-TTB is non-stoichiometric, some flexibility in the filling of PTs is a necessity. The $2\sqrt{2} \times \sqrt{2} \times 2$ structure has not been reported in previous TTB-bronze studies, and its formation may be linked to the short synthesis times employed in this work.

It must be concluded that the creation of PTs to accommodate even a small number of lead atoms gives rise to the structural distortion and the creation of the extended superlattice. Energetically, the differences between the different possible superstructures must be very slight, as indicated by the disorder in the superlattice maxima observed in some instances (Fig. 4a). The distinction between disordered superlattices and a genuinely modulated superstructure is a very fine one, but we can find no evidence here to confirm the presence of the latter. Indeed, unless the magnitude of the octahedral distortion is linked to the tunnel occupancy it is difficult to conceive of a model that would permit infinitely variable distortions in the lattice framework.

ACKNOWLEDGMENTS

The authors wish to express thanks to the E.P.S.R.C., for providing microscope facilities and financial support via grant RG29391, and to the Isaac Newton Trust and JEOL (UK) for additional financial support to SKH.

REFERENCES

1. G. Hägg, *Nature* **135,** 847 (1935); *Z. Phys. Chem. B* **29,** 192 (1935).
2. A. Magnéli, *Ark. Kemi.* **1,** 213 (1949).
3. A. Magnéli, *Acta Chem. Scand.* **7,** 315–324 (1953).
4. A. Hussain and L. Kihlborg, *Acta Crystallogr. A* **32,** 551 (1976).
5. R. D. J. Tilley, *Int. J. Refract. Metals Hard Mater.* **13,** 93–109 (1995).
6. L. A. Bursill and B. G. Hyde, *Nat. Phys. Sci.* **240,** 122 (1972).
7. B. G. Hyde and M. O'Keeffe, *Acta Crystallogr. A* **29,** 243 (1973).
8. F. Takusagawa and R. A. Jacobson, *J. Solid State Chem.* **18,** 163–174 (1976) .
9. R. Steadman, *Mat. Res. Bull.* **7,** 1143–1150 (1972).
10. M. Goreaud, Ph. Labbé, Y. Monfort, and B. Raveau, *Rev. Chim. Miner.* **17,** 79 (1980).
11. S. T. Triantafyllou, P. C. Christidis, and Ch. B. Lioutas, *J. Solid State Chem.* **130,** 176–183 (1997).
12. A. W. Sleight, *Acta Chem. Scand.* **20,** 1102–1112 (1966).
13. S. Iijima and J. G. Allpress, *Acta Crystallogr. A* **30,** 22 (1974).
14. S. Iijima and J. G. Allpress, *Acta Crystallogr. A* **30,** 29 (1974).
15. S. K. Haydon and D. A. Jefferson *J. Solid State Chem.* **161,** 135 (2001).
16. Ph. Labbé, M. Frey, and G. Allais, *Acta Crystallogr. B* **29,** 2204 (1973).
17. Ph. Labbé, M. Frey, B. Raveau, and J. C. Monier, *Acta Crystallogr. B* **33,** 2201–2212 (1977).
18. A. F. Wells, 'Structural Inorganic Chemistry,' 5th ed. Clarendon Press, Oxford, 1984.
19. R. A. Bernoff and L. E. Conroy, *J. Amer. Chem. Soc.* **82,** 6261 (1960).
20. T. Ekström and R. D. J. Tilley, *J. Solid State Chem.* **24,** 209–218 (1978).
21. M. M. Dobson, J. L. Hutchinson, R. D. J. Tilley, and K. A. Watts, *J. Solid State Chem.* **71,** 47–60 (1987).
22. D. A. Jefferson, J. M. Thomas, G. R. Millward, K. Tsuno, A. Harriman, and R. D. Brydson, *Nature* **323,** 428–431 (1986).
23. P. J. Hewitt, D. A. Jefferson, G. R. Millward, and K. Tsuno, *JEOL News* **27,** 2–9 (1989).
24. D. A. Jefferson, G. R. Millward, and J. M. Thomas, *Acta Crystallogr. A* **32,** 823 (1976).
25. T. Ekström and R. D. J. Tilley, *Chem. Scripta* **16,** 1–23 (1980).
26. M. Sundberg, *Chem. Scripta* **14,** 161–166 (1978).
27. S. K. Haydon, Ph.D. Thesis, University of Cambridge, 2000.